# Analysis of the Evolution of the Structure of a Surface With Pyramidal Asperities in Contact With a Hard and Smooth Plane

Bourassia Bensaad, Brahim Bourouga

# Analysis of the Evolution of the Structure of a Surface With Pyramidal Asperities in Contact With a Hard and Smooth Plane

**Bensaad Bourassia**
Smart Structures Laboratory (SSL), University Center of Ain Temouchent,
P.O. Box 284,
Ain Temouchent 46000, Algeria
e-mails: bourassia.bensaad@gmail.com; bourassia.bensaad@cuniv-aintemouchent.dz

**Bourouga Brahim**
Thermokinetics Laboratory,
Polytechnic School of the University of Nantes, Christian Pauc Street CS 50609,
Nantes Cedex 3 44306, France
e-mail: brahim.bourouga@polytech.univ-nantes.fr

This research deals with the evolution of the structure of the sapphire–brass interface due to the variation of contact pressure. This evolution primarily affects the essential parameters that govern the thermal contact resistance (TCR), namely, the contact point density N, the ratio of real area of contact S*, and the distance d separating the median contact planes. The combination of three measurement techniques, namely, profilometry, imaging, and mechanical characterization, was used for the purpose of investigating the structural variation of the interface. Alternatively, the TCR, which prevails at the inter-face, was estimated. Thus, the object of our study is to propose an original and new experimental approach allowing at the same time the precise measurement of the TCR and the estimate of the contact parameters of the interface studied constituting input data to the theoretical models of TCR. The estimated values given by these last are then com-pared with those measured. Through this approach, we try to open new ways of experi-mentation that would tend to reinforce the effort of TCR modeling. The results obtained showed that the roughness parameters $R_a$ and $R_q$ are independent of loading. The rough-ness $R_p$, which is considered equal to d, is sensitive to loading and has the same decreas-ing behavior under the effect of loading. The determination of S*, using the hardness testing, is even more relevant when the effective hardness $H_c$ is considered. Analysis of data for the estimation of the TCR shows that the comparisons with the reference model (Bardon) attest to the relevance of our approach.

## Introduction

The thermal contact resistance (TCR) is the capacity of the interfacial zone to transfer heat from one solid to another. This concept has attracted significant attention in the area of experimental models [1–4]. Recently, researchers have particularly focused on thermal contact, a state in which two or more systems can exchange thermal energy. In general, two types of studies have been carried out up to now: the first one is the mechanical and/or statistical aspect that describes the interface structure and thermal transfer through the real contact area and the interstitial fluid, and the second one deals with the thermal microconstriction phenomenon. Bardon's equidistant cylindrical asperity model [5], in which the mechanical and thermal aspects are thoroughly described, is widely used by the research community. Assefraoui [6] and Bensaad and Bourouga [7] used this model for the purpose of correlating two TCR values that were estimated simultaneously, one through thermal measurement and the other by mechanical and geometrical characterization of the contact surfaces. Bardon's model was further extended by Bourouga et al. [8] to dynamic contacts, such as the contact between a hot forging tool and a workpiece. An original approach was also developed and proposed by Guillot et al. [9] to easily estimate the three parameters, namely, the generated heat flux density, partition coefficient and thermal contact resistance, of the thermal contact at the interface between the tool and the workpiece in a high speed machining process. Afterward, the thermal sliding contact resistance at the tool–workpiece interface, under large strains, was investigated using an experimental approach based on temperature field measurement by thermocouples [10].

It is worth recalling that the thermal contact model, developed by Chantrenne and Sacadura, uses two essential parameters, namely, the TCR and the flux generation coefficient, in order to investigate heat transfer phenomena through dry sliding contacts [11]. For their part, Bauzin et al. performed the experimental validation of a thermal contact resistance model considering the three sliding contact parameters, i.e., roughness, velocity, and pressure [12]. On the other hand, Chern [13] used the finite element method to analyze the microtemperature of peaks and valleys of multiply asperity sliding contact surfaces. This factor has a significant effect on the contact properties, such as the chemical reactions of automatic injectors for medicine and chemical processes and surface failure of micro and macrodevices.

In order to determine the typical experimental conditions that allow minimizing the temperature loss during the glass forming process, an experimental procedure was developed by Abdulhay et al. [14] for the purpose of estimating the thermal contact resistance at the glass–metal contact interface using the Beck inverse technique. Another experimental device was developed by Abdulhay et al. [15] to estimate the thermal contact resistance at the tool—part interface during the three stages of the hot-stamping process. A correlation between the TCR and contact pressure was established in order to be used for numerical simulation.

Moreover, Black et al. [16] found a relationship between the constriction resistance, which contributes to the TCR between rough metallic surfaces, and the geometrical and thermophysical parameters. Most engineering surfaces are well represented by that correlation. Afterwards, Merrill and Garimella [17] employed a design of experiments approach to determine the effects of metallic coatings on the TCR. Later, a constriction resistance

model was combined with a surface deformation analysis based on the mechanical deformation of a coated surface previously indented with a spherical indenter. On the other hand, by putting particular focus on machined surfaces, which represent the mating surfaces in some turbo-machinery applications, Gopal et al. [18] presented an experimental work where they investigated the effect of loading and unloading history for numerous cycles.

For his part, Persson [19] discussed the crossover from the nanoscale to the macroscale and showed that, for macroscopic solids, the spreading resistance dominates the interfacial resistance in most cases. Moreover, Lishchuka [20] studied multilayered porous silicon nanostructures, fabricated by electrochemical etching of monocrystalline Si substrates, by applying a periodically changing current density. The difference between the experimental and theoretical values of thermal conductivity can certainly be attributed to the presence of thermal resistance at the interface between the porous layers.

In addition, Liu et al. [21] established a computational model with a finite element algorithm for high-temperature TCR simulation based on the multipoint contact theory. Moreover, the effects of critical parameters, such as the contact pressure, average interface temperature and equivalent surface roughness, on the thermal contact resistance with and without thermal interface materials were investigated. To enquire about the impact of the thermal contact resistance on the efficiency of cooling in cryogenic instrument, Mykhaylyk et al. [22] formulated a phenomenological model that describes the empirical relationship between various phenomena. This model systematically explains the observed power law expressing the thermal contact resistance that depends on the applied load and the roughness changes of the surfaces in contact. On the other hand, Based on the current knowledge of the surface topography and material properties of the two contacting surfaces, for a given contact pressure and apparent contact area, the numerical model developed by Vishal et al. [23] can be used to predict the thermal contact resistance.

Other models dealing specifically with mechanical aspects, such as elastic, plastic, and elasto-plastic mechanical patterns of contact, have been employed as well. Greenwood and Williamson's model [24] is among the most widely used models, in which the authors made an important number of hypotheses, i.e., deformations are either purely elastic or purely plastic. One can draw from this model the conclusion that in the elastic case the real contact area is proportional to loading. The model of Whitehouse et al. [25] remains close to Greenwood and Williamson's model but they differ in the hypotheses made on the constant radius and the choice of the Gaussian distribution of asperity heights. Cooper et al. [26] proved, through a theoretical and experimental study, that the thermal transfer at the interface is crucially dependent on the distribution of the highest peaks on the surface and for this reason the Gaussian distribution becomes suspect. Inspired by Bowden and Tabor's model [27] for plastic deformation, Yovanovich [28] proposed a new one that expresses the contact parameters as a function of the effective microhardness $H_c$, which is in turn, is expressed in terms of the apparent contact pressure and surface roughness parameters. The authors highlighted the effect of hardening on the real contact. It is worth noting that Bowden and Tabor considered that the real contact pressure is equal to the material's hardness at the summit of the asperity. Mikic [29] proposed a thermal conductance model that considers the cases of pure plastic deformation, plastic deformation of asperities, elastic deformation of substrate, and pure elastic deformation. Considering that the transition from one deformation mode to another cannot be a simple "switchover" action, Sridhar and Yovanovich [30] proposed an elasto-plastic model based on that of Cooper et al. [26].

The present experimental work aims to study the simultaneous evolution of the contact parameters at the sapphire–metal interface, under progressive loading, and the thermal contact resistance. The object of our study is to propose an original and new experimental approach allowing at the same time the precise measurement of the TCR and the estimate of the contact parameters of the interface studied constituting input data to the Bardon's theoretical model of TCR [5]. The estimated values given by these last are then compared with those measured. Through this approach, we try to open new ways of experimentation that would tend to reinforce the effort of TCR modeling.

**Table 1 Roughness of surfaces with pyramidal asperities**

| | LP3 | LP4 | LP5 |
|---|---|---|---|
| $c$ ($\mu$m) | 330 | 252 | 140 |
| $h$ ($\mu$m) | 90 | 77 | 50 |

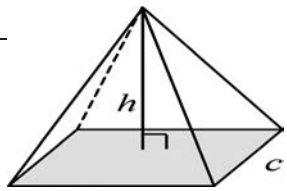


It was decided to use a combined measurement technique in which one could, on the one hand, observe by optical profilometry, imaging, and mechanical characterization the changes of the interface structure and on the other hand measure the TCR in steady regime.

The results obtained for surfaces with pyramidal asperities were recorded.

## Experimental Approach

The main idea was to estimate the interface parameters that allow evaluating the TCR from profilometric analyses or imaging [7]. These parameters are the ratio of real area of contact $S^*$, the density of contact points $N$, and the height $d$ of the highest peak. One considers the favorable case of a plane contact between a smooth and infinitely rigid surface (sapphire) and another rough and deformable one made of brass. This interface was subjected to progressive loading. The density of contact points $N$ was evaluated from the processing of the sample surface images obtained by direct photography through the transparent wall of sapphire. The interface was then filled with an opaque paste. The separation distance between median planes was determined from the topographies recorded after each loading step. Moreover, $S^*$ was determined from measurements of the contact pressure and microhardness of the sample. In order to take into account the work hardening phenomenon, the microhardness was measured for the entire field of values of the applied force. The movement of matter that causes the increase in the actual surface area of contact was also investigated. On the other hand, the thermal resistance was simultaneously measured on steady-state. The TCR values obtained were then systematically compared with the estimated values using a specific theoretical model.

Three different specimens, whose dimensions are summarized in Table 1, were considered for the purpose of studying the evolution of the TCR as a function of the number $N$. The brass specimens with pyramidal indentations on the surface were designated by (laiton (brass) pyramid) LP.

## Measuring Apparatus

The five main elements of the experimental apparatus shown in Fig. 1 are the following: the sapphire (1), the brass or steel sample with thermocouples (5), the heater (3), the cold box (4), and the pneumatic loading system (7) [7]. The electric heater constituting the hot source is mounted on a poorly conductive seat (11). In order to obtain a good contact, a thin conductive layer of graphite grease is put on the interface between the sample and the heater. The water box (cold source) is arranged in perfect contact with the sapphire. The very smooth surfaces of the sapphire and water box are coated with graphite grease to improve thermal contact. In fact, the water box comes to replace the crown carrying the viewing window as shown in Fig. 1. It is traversed by a thermally controlled flow of water and thus serves to maintain a temperature

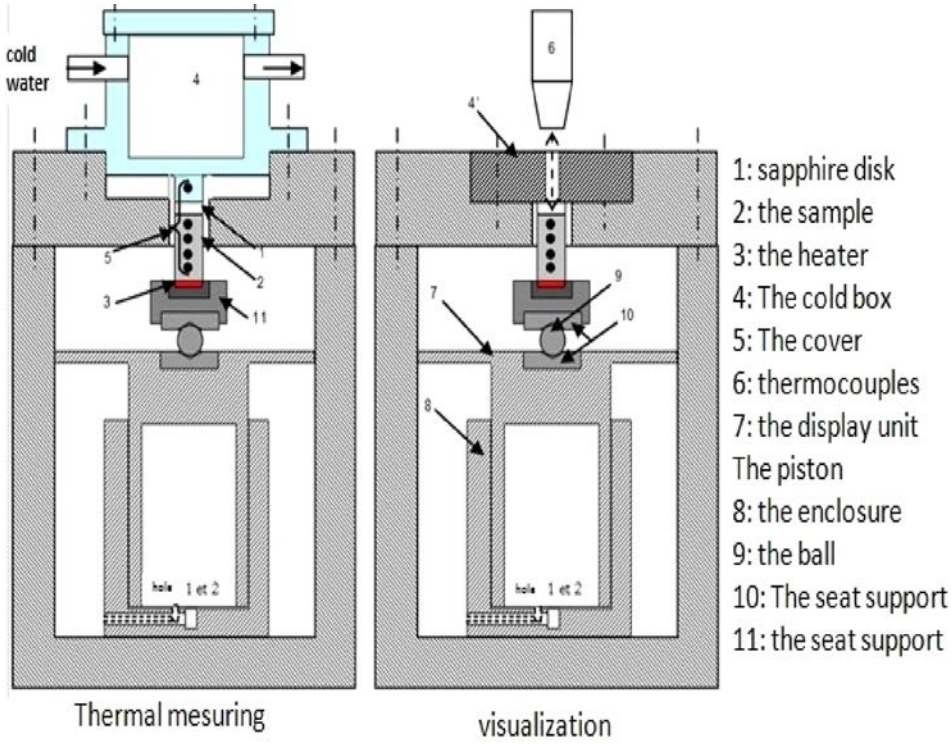


**Fig. 1 Sketch of measurement system**

gradient along the axis of symmetry. The applied heating has for reference the ambient temperature. Thus, the temperature of the cold source is maintained equal to the latter by a flow of thermoregulated water through the cold box by means of a Lauda RK20 type apparatus (Thermokinetics Laboratory, Polytechnic School of the University of Nantes, Nantes, France). Before activating the hot source, it is verified that all the thermocouples both in the sample and in the wall of the cold box give a single temperature: the ambient temperature.

The sapphire—sample—heater assembly is mounted on a conical seat (10) carried by a steel ball (9). The pneumatic load force combined with this type of support is used to avoid partial contact at the interface.

The contact between the specimen and the sapphire is made using setup screw mounted on the piston plate. The latter is backed up by the edge of the thick wall of the cylinder. Once the contact is made a low load is applied to the cylinder. We can then proceed to the pressure setup by means of the regulator installed at the exit of compressed air circuit or by a throttle placed before in the pressured air circuit. The assembly is then aligned under the effect of load.

The samples are of cylindrical form with 8 mm in diameter and 10 mm in height. Figure 1 shows that each specimen is equipped along its axis by four thermocouples of K type welded at the bottom of the radial holes of 0.5 mm in diameter. The distances of welds to the interface are 1.5, 3.5, 5.5, and 7.5 mm, respectively. The plate of sapphire has the form of a polished disk of 8 mm in diameter and 2 mm in thickness. Its two faces are polished and have a roughness $R_a$ of 30 nm. The total assembly is mounted aligned in a system associated with the pneumatic loading system. This system is mainly a cylinder of 60 mm in height and 95 mm in diameter equipped with a rigid piston to support the air pressure of 6 bar. Two holes are made in the cylinder wall, the first is used for pressured air input and the second holds a pressure sensor of Kisler XT-190M-7-BAR-G type, which is linked to a conditioner type AW180-A10S-FN with analog output of 0–10 V in continuous electric current. A hard steel doughnut of 20 mm in thickness is mounted on the pneumatic system, which allows mounting the different accessories required for thermal measurement and interface visualization. The thermocouples and pressure sensor responses are registered through a data acquisition chain.

To identify the surface finish of the specimens, a profilometer UBM type UBC14 with dynamic focalization is used. Its definition is 0.5 $\mu$m in the plan of the surface and 6 nm in the normal direction. With the visualization cell represented in Fig. 1, the interface sapphire–metal is loaded up to the chosen contact pressure in order to perform the contact thermal resistance measurement. A special mounting allows observing and photographing the interface through a window of 3 mm in diameter. The photography is made by a digital camera mounted on a stereo-microscope Olympus K700 providing a zoom from 6 to 50×. The camera allows supplementary zoom of 1.25×. The camera is controlled by a personal computer. A code of image analyzer allows determining the number of contact points.

## Experimental Procedure

Figure 2 gives a schematic of an experiment for a given specimen. We note that microhardness test is a series of measures made for different values of applied loads. For each value of load, seven indentations are made and the average value is used to plot the curve of microhardness.

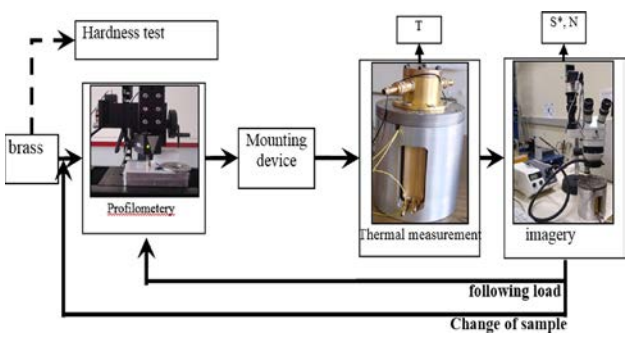


**Fig. 2 Diagram summarizing the course of the experience of a given sample**

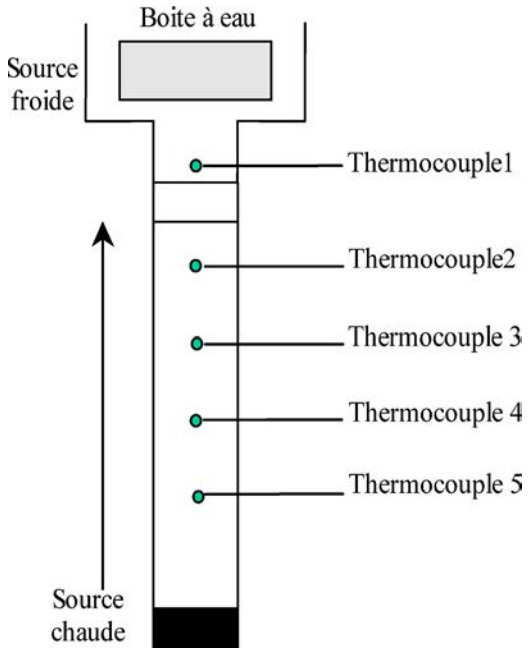


**Fig. 3 Schematic diagram**

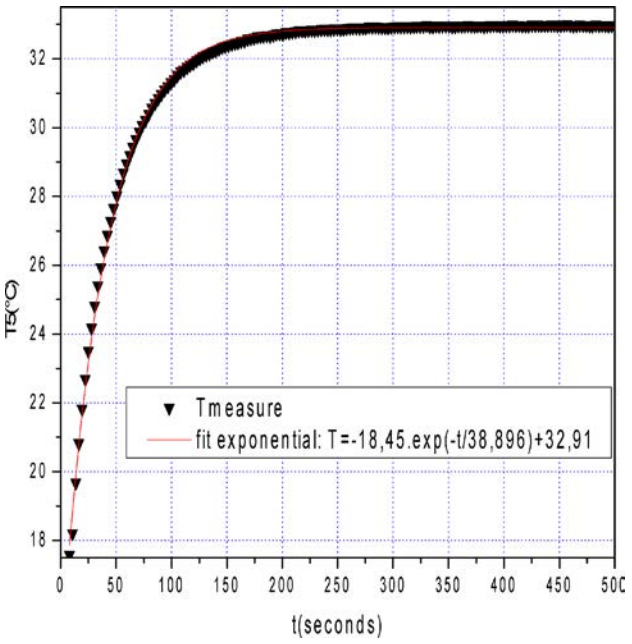


**Fig. 5 Measurement of the time constant on a temperature record for the sapphire/LP3 pair**

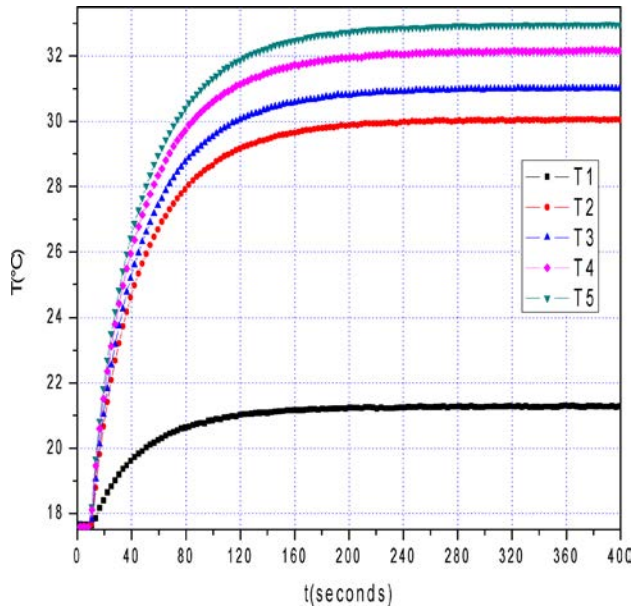


**Fig. 4 Example of temperature recording, experiment on sample LP3 with contact pressure 148.9 bar**

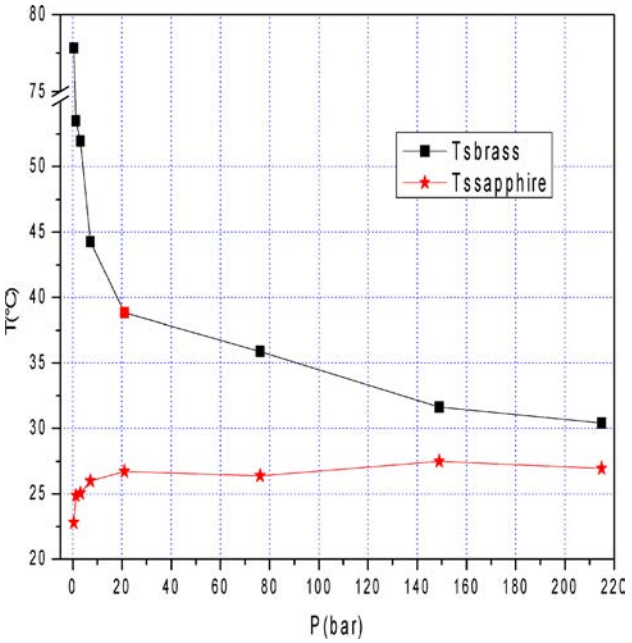


**Fig. 6 Example of sapphire and brass surface temperature values, sample LP3**

## Thermal Contact Resistance Calculation

**Thermal Measurement.** In Fig. 3, we recall the positions of the five thermocouples used in this study. For each measurement, we record the temperature fields during the heating of the sapphire–metal sample pair under an applied mechanical load. In Figs. 4 and 5, we present the raw temperature records obtained during an experiment on the LP3 sample under the maximum load of 148.9 bar.

### The Determination of the Thermal Contact Conditions

*Surface Temperatures and Heat Flow at the Contact.* For steady regime, the measurements taken by the thermocouples T2, T3, T4, and T5 draw a linear curve which makes it possible to determine the value of the temperature at the face of the sample participating to the contact.

Knowing the density of heat flow through the interface of the contact and the temperature measured by the thermocouple No. 1 and considering a perfect contact between the cold box and the sapphire, the linear law describing the temperature field makes it possible to determine the temperature of the sapphire at the interface. In Fig. 6, we present an example of sapphire and brass surface temperature values. Figure 7 presents an example of the calculated values of heat flux through the interface.

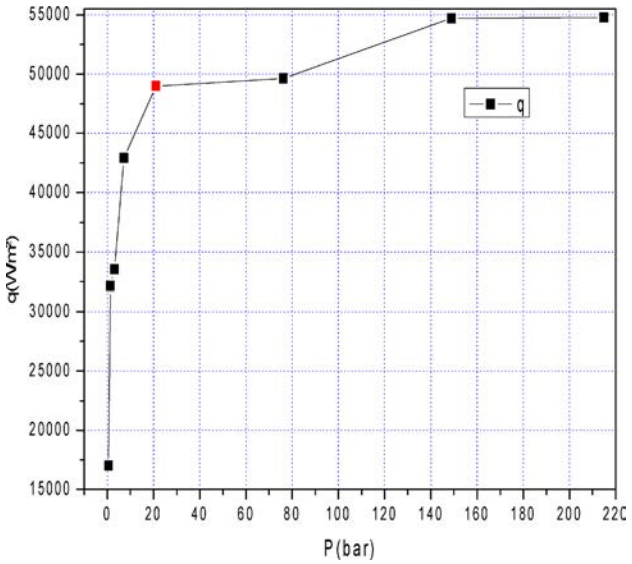


**Fig. 7 Example of values of heat flux through the interface, experiment on sample LP3**

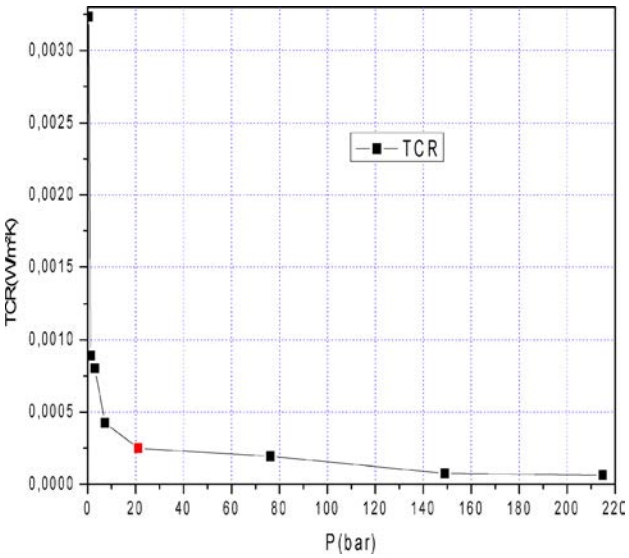


**Fig. 8 Example of values of TCR, experiments on sample LP3**

*Thermal Contact Resistance*. The principle of measuring of the thermal contact resistance consists of two steps:

- In the first step, the flow density transferred to the interface and the sample-side contact temperature $T_{\text{sbrass}}$ is estimated from the temperature measurements taken along the axis of the sample (Fig. 3).
- And in the second step, from the knowledge of the flow density that crosses the interface and that of the temperature given by the thermocouple implanted in the brass wall of the cold box (Fig. 3) supposed in perfect contact with the sapphire, one determines the sapphire side surface temperature Tssapphire.

Thus, we know the flux density $q$, which passes through the sample–sapphire interface and the two temperatures of the surfaces in contact $T_{\text{sbrass}}$ and $T_{\text{ssapphire}}$. The contact resistance can then be determined from the following ratio:

$$\text{TCR} = \frac{T_{\text{sbrass}} - T_{\text{ssapphire}}}{q} \tag{1}$$

Figure 8 presents an example of the calculated values of the thermal contact resistance.

## The Estimation of the Thermal Contact Resistance

It is considered that the TCR results from the parallel composition of two resistors $R_s$ and $R_f$, where

- $R_s$ is the resistance to the passage of the heat flux by solid–solid direct contact, it is calculated by the Bardon's model.
- and $R_f$ is the resistance to the passage of heat flow through the interstitial medium fluid.

One can estimate the TCR as

$$\text{With} : \frac{1}{\text{TCR}} = \frac{1}{R_s} + \frac{1}{R_f} \leftrightarrow \text{TCR} = R_s R_f / (R_s + R_f) \tag{2}$$

## Results and Discussion

**Analysis of Deformation Data and Contact Parameters.** The mechanical deformations to which the rough surface of the specimen is subjected cannot be seen through the sapphire wall under loading using the profilometer [7]. Indeed, Assefraoui [6], who had developed a similar device with a lever-loading system, noticed that such an experiment gives very erroneous results due to an optical deformation of the topography that is induced by the presence of sapphire. After checking this result, it turned out that only the plastic deformations of the surface before and after the loading, without the presence of sapphire, could be considered. For the profilometric measurements, only an increment of 1 $\mu$m was used, as recommended by Assefraoui. It was revealed from the experiment that a square surface with twelve pyramids can be representative of the total base surface of the specimen under study. The surface texture was also statistically characterized. Figure 9 and Table 2 indicate that the pyramidal surfaces are not Gaussian. Figure 10 indicates that the roughness parameters $R_a$ and $R_q$ are independent from loading. However, the roughness $R_p$, which is considered equal to $d$, is very sensitive to loading.

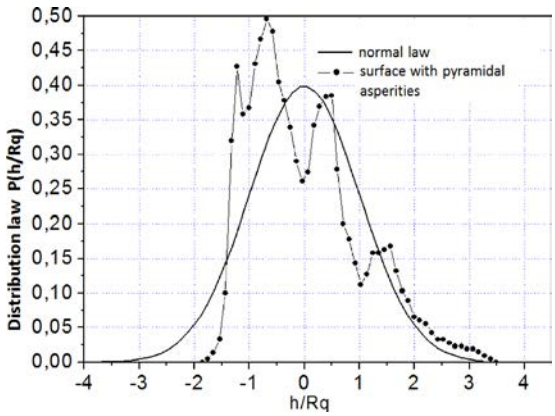


**Fig. 9 Comparison of the normal law and distribution law of investigated surfaces**

**Table 2 Statistical characteristics of surfaces**

| | $m_1$ | $R_a$ ($\mu$m) | $R_q$ ($\mu$m) | $S_k = m_3/R_q^3$ | $K = m_4/R_q^4$ |
|---|---|---|---|---|---|
| Normal law | 0 | — | — | 0 | 3 |
| Controlled surface | 0.13 | 8.8 | 10.8 | −0.78 | 4.8 |

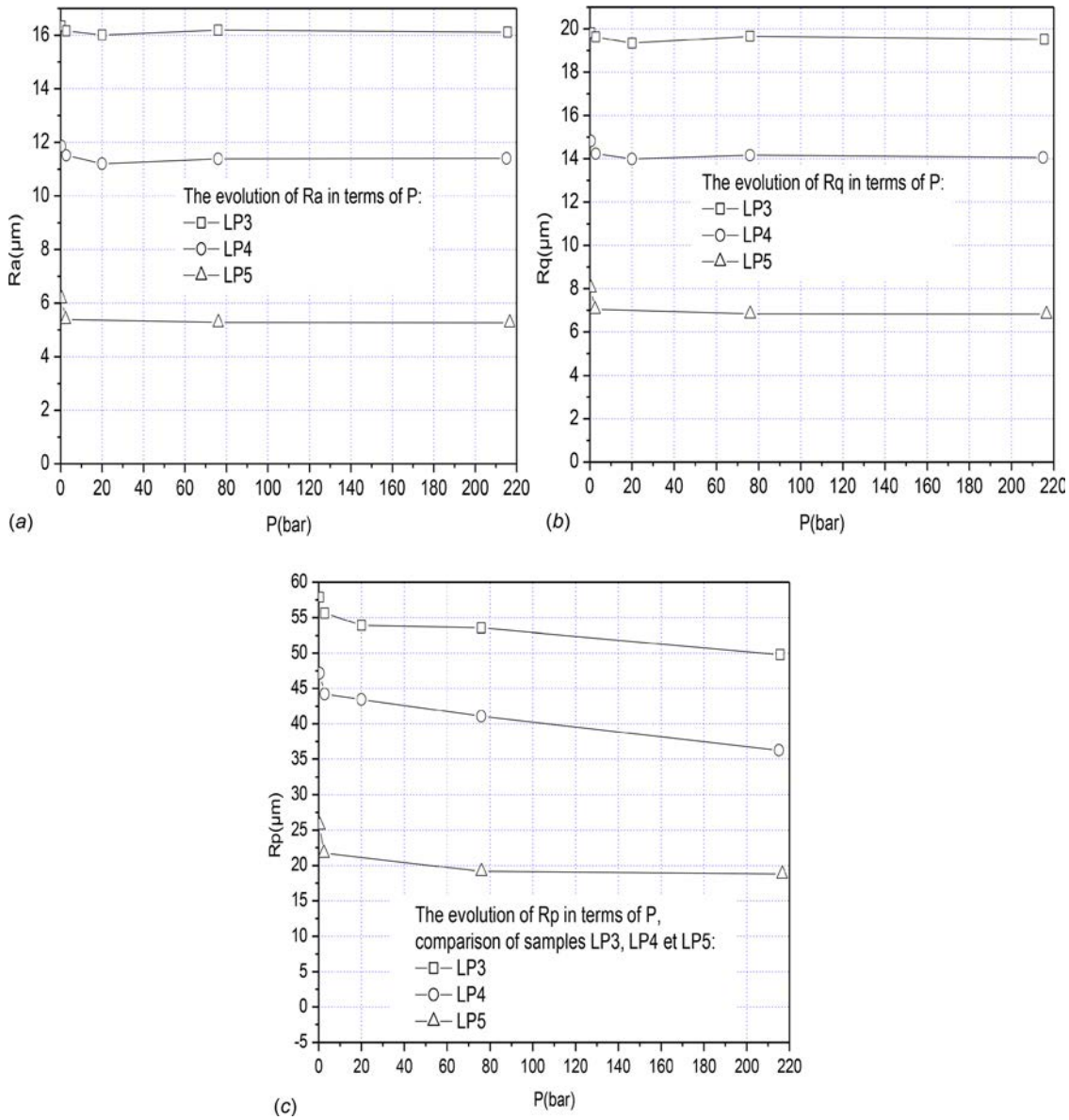


**Fig. 10 Evolution of roughness parameters $R_a$ (*a*), $R_q$ (*b*), and $R_p$ (*c*) as a function of the load $P$**

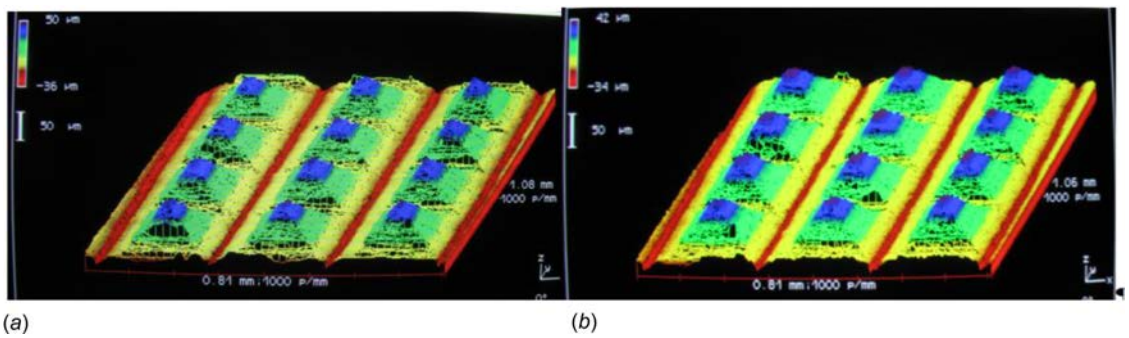


**Fig. 11 View of the sample before and after loading: (*a*) before loading and (*b*) after loading ($P = 78$ bar)**

Figure 11 clearly demonstrates that the pyramidal asperities present different peaks and the surface has a *nonuniform roughness*. In addition, the color contrast in Fig. 11(*b*) indicates that the pyramid summits are crushed and flattened, and therefore, the total roughness goes from 86 $\mu$m before crushing to 76 $\mu$m after crushing. It is observed from profilometry that the heights of the different pyramids are not equal; they show an average dispersion of 5 $\mu$m. This has an impact on $N$, which is minimum for a load level of 0.5 bar. Then $N$ starts increasing with $P$ to eventually reach a maximum value, which is confirmed by Fig. 12.

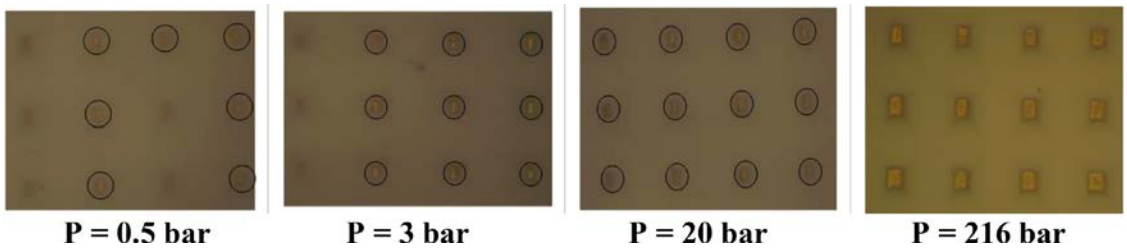


**Fig. 12 Images of the interface between asperities and sapphire depending on the load**

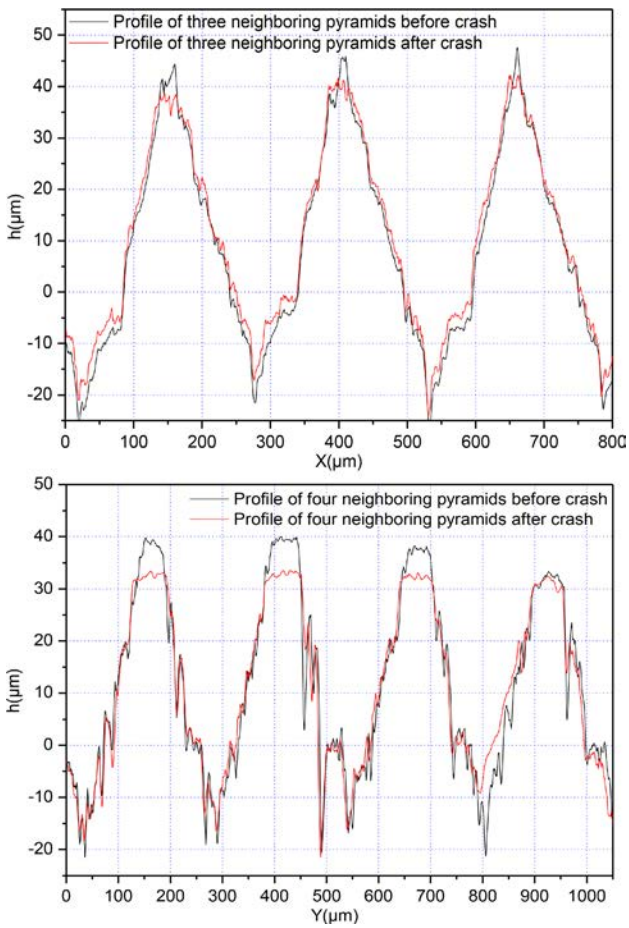


**Fig. 13 Topographic profiles of the rough surface, measured along *Ox* and *Oy*, before and after loading (*P* = 78 bar)**

Obviously, the flow of matter and hardening should be different from one pyramid to another. Furthermore, Fig. 13 presents the profiles passing by the summits of asperities along the *Ox* and *Oy* axes. Note that the highest peaks were reduced after crushing. It is important to mention that the scan increment, i.e.,1 $\mu$m, is very small and it is difficult to find the accurate profile before deformation. The width of the first pyramid was measured at the ordinate of 30 $\mu$m; its width before crushing was 53 $\mu$m and then it increased by 5 $\mu$m after a loading of 78 bar as seen on the profile's superposition along *Ox*. The decrease in altitude and widening of the top of the pyramid can be observed on the profile, along *Oy*. At the altitude of 33 $\mu$m, which corresponds to the ordinate of 30 $\mu$m, the width varies between 55 $\mu$m and 66 $\mu$m. The average deformation represented by the variation of the total roughness is, in this case, about 6 $\mu$m or 7 $\mu$m. Furthermore, different machining defects were observed along the *Ox* and *Oy* directions. The observation of the two profiles shows the presence of a second roughness scale (3–4 $\mu$m). This is valid for the twelve pyramids studied.

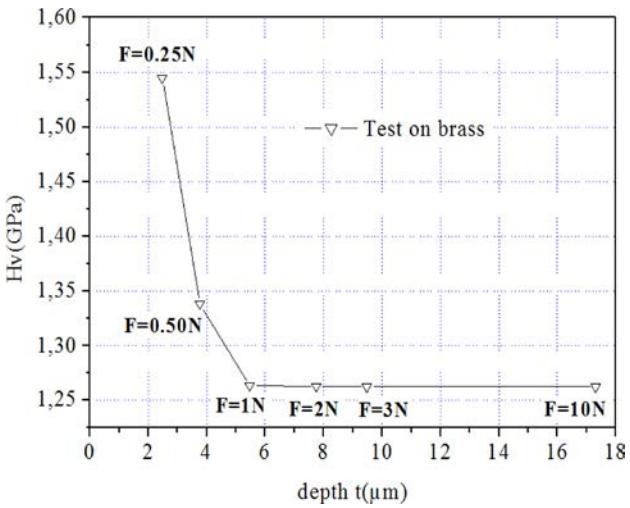


**Fig. 14 Vickers hardness test**

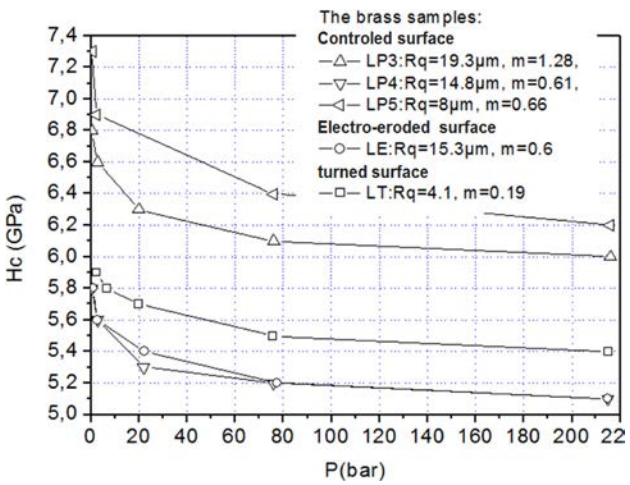


**Fig. 15 Effective microhardness plots**

**Mechanical Characterization of the Interface.** The Vickers hardness test was carried out on brass, as shown in Fig. 14; it can easily be noted that for a load of 100 g, the hardness is constant and is equal to 1.26 GPa, which is about 16 times lower than sapphire hardness (20 GPa). This confirms the hypothesis that sapphire is dimensionally stable. The Vickers microhardness values for brass are dependent on the penetration depth as shown in Fig. 14. The points shown represent the average value of 6 test values at each load.

Initially, $S^*$ was estimated by means of the Bowden and Tabor's model [27] using the Vickers microhardness $H_v$; then, the effect of hardening phenomenon on the real contact was taken

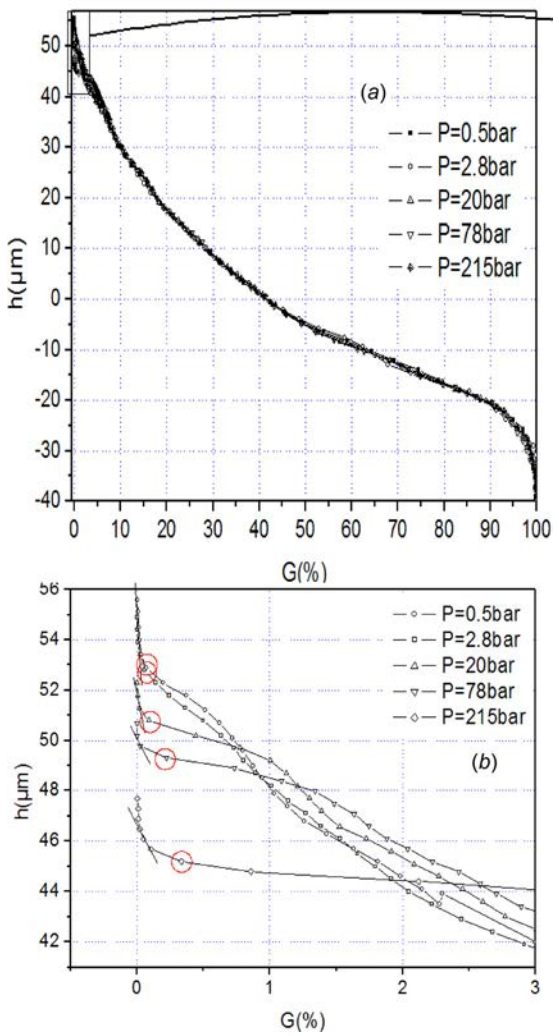


**Fig. 16 (*a*) Abbott curves recorded after loading (*b*) top of the pyramid in (*a*)**

into account, and $H$ was considered as equal to the effective microhardness obtained by Yovanovich's model [28]. Therefore, it may be said that The effective microhardness is quite original as it combines the microhardness test results with those of the profilometric measurements. Figure 15 explicitly indicates that $H_c$ is five times greater than $H_v$.

**Analysis of Data for the Estimation of $S^*$.** Initially, $S^*$ was estimated by means of the Bowden and Tabor's model [27] using the Vickers microhardness $H_v$ ($S^*_{Hv}$); then, the effect of hardening

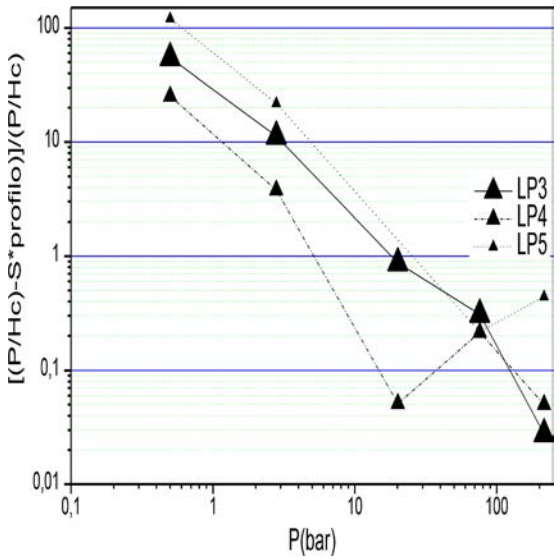


**Fig. 17 The variation of the difference between "$S^*_{profile}$" and "$S^*_{Hc}$" with respect to "$S^*_{Hc}$" according to the loading**

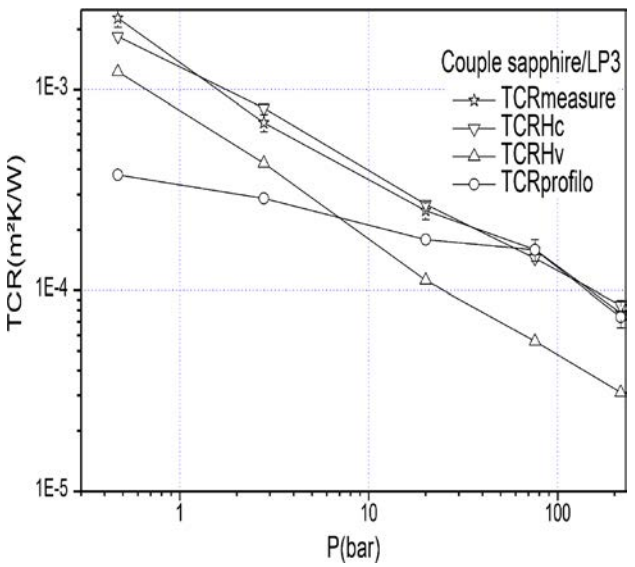


**Fig. 18 Thermal contact resistance values measured and estimated in terms of $S^* = P/H_c$, $S^* = P/H_v$ and $S^*_{profilo}$, couple sapphire/LP3**

**Table 3 Values of $S^*$(%) for the sapphire–brass pair**

| | $P$ (bar) | 0.5 | 2.8 | 20.1 | 75.9 | 215.6 |
|---|---|---|---|---|---|---|
| Couple sapphire/LP3 | $S^* = P/H_v$ | 0.004 | 0.02 | 0.16 | 0.6 | 1.7 |
| | $S^* = P/H_c$ | 0.0007 | 0.004 | 0.032 | 0.12 | 0.36 |
| | $S^*_{\text{profilo}}$ | 0.039 | 0.049 | 0.06 | 0.083 | 0.35 |
| Couple sapphire/LP4 | $S^* = P/H_v$ | 0.004 | 0.022 | 0.17 | 0.6 | 1.7 |
| | $S^* = P/H_c$ | 0.0008 | 0.0048 | 0.039 | 0.14 | 0.4 |
| | $S^*_{\text{profilo}}$ | 0.021 | $2.3 \times 10^{-2}$ | $3.7 \times 10^{-2}$ | 0.11 | 0.42 |
| Couple sapphire/LP5 | $S^* = P/H_v$ | 0.0037 | 0.02 | — | 0.60 | 1.7 |
| | $S^* = P/H_c$ | 0.00065 | 0.0035 | — | 0.12 | 0.34 |
| | $S^*_{\text{profile}}$ | $7.9 \times 10^{-2}$ | $8 \times 10^{-2}$ | | $9.4 \times 10^{-2}$ | 0.19 |

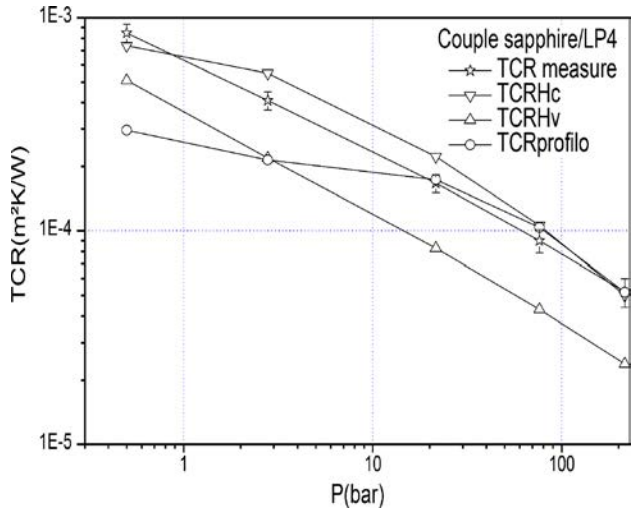


**Fig. 19 Thermal contact resistance values measured and estimated in terms of $S^* = P/H_c$, $S^* = P/H_v$ and $S^*_{profilo}$, couple sapphire/LP4**

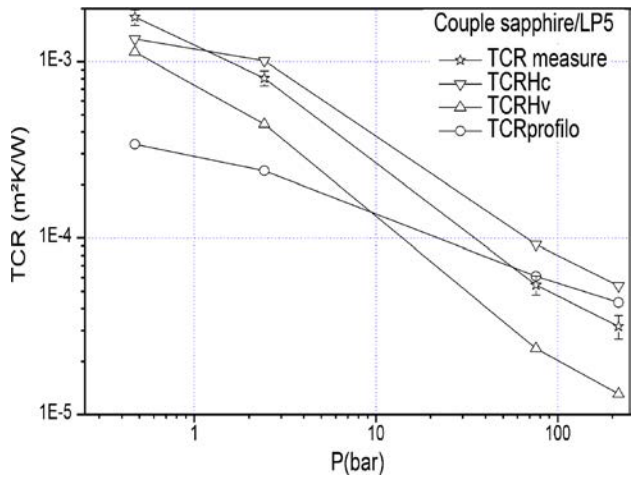


**Fig. 20 Thermal contact resistance values measured and estimated in terms of $S^* = P/H_c$, $S^* = P/H_v$ and $S^*_{profilo}$, couple sapphire/LP5**

phenomenon on the real contact was taken into account, and $H$ was considered as equal to the effective microhardness obtained by Yovanovich's model [28] ($S^*_{Hc}$).

The values of $S^*$ obtained by profilometry ($S^*_{profilo}$) are considered as equal to the bearing rate $G$ corresponding to the first point taken after the change of slope of the Abbott curve observed at the summit of the asperity, as illustrated in Fig. 16. Table 3 displays the values of $S^*$ for each specimen.

The Fig. 17 shows the variation of the difference between "$S^*_{profilo}$" and "$S^*_{Hc}$" with respect to "$S^*_{Hc}$" according to the loading. The analysis shows that using $H_v$ gives values of $S^*$ higher than those obtained through $H_c$. For large loads, the values of $S^*_{profilo}$ are closer to those estimated through the use of $H_c$.

In order to determine the most relevant estimation, it was decided to proceed to the evaluation of the thermal contact resistance by the model of Bardon [5] and then compare it with the one obtained by thermal measurement.

**Analysis of Data for the Estimation of the Thermal Contact Resistance.** We note that the reproducibility study of the estimate of the contact resistance TCR shows that the levels of value of TCR and its dispersion attest to the good reliability of the measuring device [7].

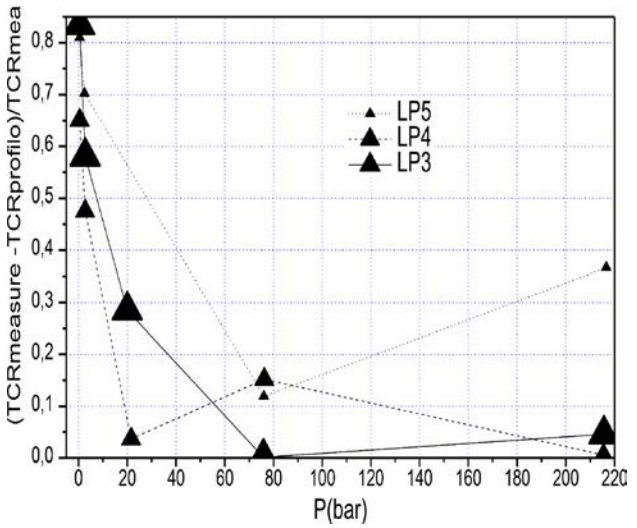


**Fig. 21 The variation of the difference between "$TCR_{profilo}$" and "$TCR_{measure}$" with respect to "$TCR_{measure}$" according to the loading**

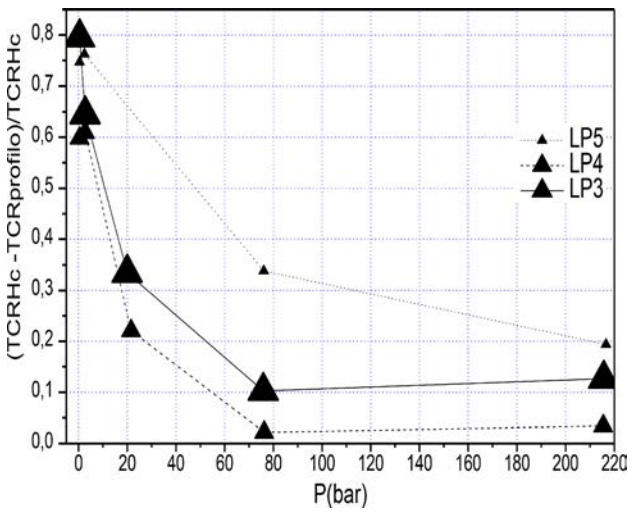


**Fig. 22 The variation of the difference between "$TCR_{profilo}$" and "$TCR_{Hc}$" with respect to "$TCR_{Hc}$" according to the loading**

Figures 18–20 show the comparison between the measurement of the TCR and its estimation as a function of "$S^*_{Hc}$," "$S^*_{Hv}$," and "$S^*_{profile}$." We observe that the determination of $S^*$ using the hardness test results is relevant and particularly when considering the effective hardness $H_c$. It allows noting that for larger loads, the estimated value is close to that measured; the relative difference hardly exceeds 4% especially for samples LP3 and LP4.

Figure 21 shows that the difference between the estimation of the TCR as a function of "$S^*_{profilo}$" and "$TCR_{measure}$" is very important for the low loads. This difference decreases by increasing the load. From a load of 20 bar it does not exceed 30% of the measurement. Figure 22 shows that the difference between the estimation of the TCR as a function of "$S^*_{profilo}$" and that as a function of "$S^*_{Hc}$" is very important for the low loads. This difference decreases by increasing the load. From a load of 20 bar it does not exceed 35% of the estimated value of the TCR as a function of "$S^*_{Hc}$."

For low loads, the assumption that $S^*$ is equal to the bearing rate $G$ leads to underestimate the TCR. This can be justified by the spring back of the material, at the top of the

asperity, and/or by the presence of the second scale of roughness observed.

## Conclusion

The basic idea of this research was to estimate the interface parameters $S^*$, $N$, and $d$ that allow determining the thermal contact resistance from profilometric analyses or imaging. The surface with identical pyramidal asperities is used to overcome the knowledge of the density of contact points which is equal to the number of pyramids per unit area. This allows to study the evolution of the real contact rate during step loading.

A contact plane was considered between a smooth and infinitely rigid material (sapphire) and a rough and deformable material (brass). This interface was subjected to progressive loading. For the purpose of taking into account the work hardening phenomenon, the microhardness was measured for all the field of values of the applied force. At the same time, the thermal resistance was measured. The TCR values measured on steady-state were systematically compared with the values estimated from the chosen theoretical model. The reproducibility of the estimate of the contact resistance TCR is studied. The levels of value of TCR and its dispersion attest to the good reliability of the measuring device.

The most important results are summarized in the following: The roughness parameters $R_a$ and $R_q$ are indifferent to loading. However, the roughness parameter $R_p$, which is considered as equal to $d$, is sensitive to loading and has the same decreasing behavior under the effect of loading. The determination of $S^*$ by hardness testing is pertinent and particularly when the effective hardness $H_c$ is taken into account. Using the model of Bardon allows giving a good estimate of the TCR.

For low loads, the differences between the $\mathrm{TCR} = f(S^*_{\mathrm{profilo}})$ and "$\mathrm{TCR}_{\mathrm{measure}}$" and that between the $\mathrm{TCR} = f(S^*_{\mathrm{profile}})$ and $\mathrm{TCR} = f(S^*_{Hc})$ are very important for the low loads. These differences decrease by increasing the load. The assumption that $S^*$ is equal to the bearing rate $G$ leads to underestimate the TCR. This can be justified by the spring back of the material, at the top of the asperity, and/or by the presence of the second scale of roughness observed.

For moderate and larger loads, the estimated values of TCR as function of "$S^*_{\mathrm{profilo}}$" and "$S^*_{Hc}$" are close to that measured, especially for samples LP3 and LP4. We conclude that the hypothesis of the plastic behavior assumption of the asperities is verified, especially for moderate and large loads.

The interesting and relevant comparisons with the reference model attest to the relevance of the approach and are encouraging to persevere in the development of new techniques for characterizing contact parameters.

## Nomenclature

$c$ = length of the side of the side of the base of the pyramid
$d$ = distance between planes of surfaces in contact ($\mu$m)
$d^*$ = normalized distance between planes of surfaces in contact ($\mu$m)
$h$ = height ($\mu$m)
$H_{\mathrm{B}}$ = Brinell hardness (GPa)
$H_c$ = effective microhardness (GPa)
$K$ = Kurtosis
$m$ = slope of asperity
$N$ = density of contact points ($\mathrm{m}^{-2}$)
$P$ = pressure (bar)
$R_a$ = arithmetic average roughness ($\mu$m)
$R_f$ = resistance solid–fluid–solid
$R_p$ = height of highest peak ($\mu$m)
$R_q$ = average quadratic roughness ($\mu$m)
$R_s$ = constriction resistance solid–solid ($\mathrm{K\,m^2/W}$)
$R_t$ = total roughness ($\mu$m)
$S^*$ = real contact ratio
$S_k$ = skewness
$T$ = temperature (K)

## References


[1] Madhusudana, C. V., 2014, *Thermal Contact Conductance*, Springer, Berlin.
[2] Yovanovich, M. M., 2005, "Four Decades of Research on Thermal Contact, Gap, and Joint Resistance in Microelectronics," IEEE Trans. Compon. Packag. Technol., **28**(2), pp. 182–206.
[3] Kumkum, M., Chauhan, B., and Raiyani, H. R., 2017, "The Parameters Affecting on Thermal Contact Conductance-A Review," Int. J. Adv. Eng. Res. Develop., **4**(3), pp. 404–410.
[4] Abdollahi, H., Shahraki, S., and Motahari-Nezhad, M., 2017, "A Review on the Effects of Different Parameters on Contact Heat Transfer," Thermophys. Aeromechanics, **24**(4), pp. 499–512.
[5] Bardon, J. P., 1972, "Introduction à L'étude Des Résistances Thermiques de Contact," Int. J. Thermal Sci., **125**, pp. 429–446.
[6] Assafraoui, A., Bardon, J.-P., and Danes, F., 1998, "Détermination de la RTC Par Analyse Profilométrique de la Déformation D'une Surface à Rugosité Pyramidale," Colloque annuel-SFT, Marseille, France, Vol. 6, pp. 79–84.
[7] Bensaad, B., and Bourouga, B., 2008, "Etude de L'évolution de la Structure D'interface de Contact Saphir-Laiton," 1ère Conférence Internationale Sur la Conversion et la Maîtrise de l'énergie, Sousse, Tunisie, Apr. 11–13.
[8] Bourouga, B., Goizet, V., and Bardon, J.-P., 2002, "Modèle Prédictif de Résistance Thermique de Contact Dynamique Adapté au Cas de L'interface Pièce-Outil de Forgeage," Int. J. Heat Mass Transfer, **46**(3), pp. 565–576.
[9] Guillot, E., Bourouga, B., Garnier, B., and Brocail, J., 2008, "Measurement of the Thermal Contact Parameters at a Workpiece—Tool Interface in a HSM Processes," Int. J. Mater. Form., **1**(Suppl. 1), pp. 1419–1422.
[10] Bourouga, B., Guillot, E., Garnier, B., and Dubar, L., 2010, "Experimental Study of Thermal Sliding Contact Parameters at Interface Seat of Large Strains," Int. J. Mater. Form., **3**(Suppl. S1), pp. 821–824.
[11] Chantrenne, P., Raynaud, M., and Sacadura, J.-F., 1996, "Détermination Des Paramètres D'un Modèle Thermique du Contact Sec Glissant: Application Aux Roulements en Ambiance Cryogénique," Proceeding du Congrés SFT1995, Vol. 3, Elsevier, Amsterdam, The Netherlands, pp. 675–680.
[12] Bauzin, J. G., Laraqi, N., and Baïri, A., 2008, "Estimation of Thermal Contact Parameters at the Interface of Two Sliding Bodies," J. Phys.: Conf. Ser., **135**, p. 012015.
[13] Chern, S. Y., Horng, J. H., Tsai, C. H., and Tsai, H. J., 2018, "The Micro-Temperatures of the Peaks and Valleys of Sliding Rough Surfaces," Appl. Mech. Mater., **883**, pp. 53–62.
[14] Abdulhay, B., Bourouga, B., Alzetto, F., and Challita, C., 2016, "Experimental Approach for Thermal Parameters Estimation During Glass Forming Process," AIP Conf. Proc., **1769**(1), p. 040003.
[15] Abdulhay, B., Bourouga, B., and Dessain, C., 2012, "Thermal Contact Resistance Estimation: Influence of the Pressure Contact and the Coating Layer During a Hot Forming Process," Int. J. Mater. Form., **5**(3), p. 183.
[16] Black, A. F., Singhal, V., and Garimella, S. V., 2004, "Analysis and Prediction of Constriction Resistance for Contact Between Rough Engineering Surfaces," CTRC Research Publications, Purdue, UK, p. 296.
[17] Merrill, C., and Garimella, S. V., 2011, "Measurements and Prediction of Thermal Contact Resistance Across Coated Joints," CTRC Research Publications, Purdue, UK, p. 235.
[18] Gopal, V., Whiting, M. J., Chew, J. W., and Mills, S., 2013, "Thermal Contact Conductance and Its Dependence on Load Cycling," Int. J. Heat Mass Transfer, **66**, pp. 444–450.
[19] Persson, N. J., 2014, "Thermal Interface Resistance: Cross-Over From Nanoscale to Macroscale," J. Phys.: Condens. Matter, **26**(1), p. 015009.
[20] Lishchuk, P., Dekret, A., Pastushenko, A., Kuzmich, A., Burbelo, R., Belarouci, A., Lysenko, V., and Isaiev, M., 2018, "Interfacial Thermal Resistance Between Porous Layers: Impact on Thermal Conductivity of a Multilayered Porous Structure," Int. J. Therm. Sci., **134**, pp. 317–320.
[21] Liu, D., Zhang, J., and Wang, X.-D., 2018, "Numerical Simulation of High-Temperature Thermal Contact Resistance and Its Reduction Mechanism," PLoS One, **13**(3), p. e0194483.
[22] Mykhaylyka, V. B., Burt, M., Ursachi, C., and Wagner, A., 2012, "Thermal Contact Conductance of Demountable in Vacuum Copper-Copper Joint Between 14 and 100 K," Rev. Sci. Instrum., **83**(3), p. 034902.
[23] Singhal, V., Litke, P. J., Black, A. F., and Garimella, S. V., 2005, "An Experimentally Validated Thermo-Mechanical Model for the Prediction of Thermal Contact Conductance," Int. J. Heat Mass Transfer, **48**(25–26), pp. 5446–5459.
[24] Greenwood, J. A., and Williamson, J. B. P., 1966, "Contact of Nominally Flat Surfaces," Proc. R. Soc. A, **295**(1442), pp. 300–319.
[25] Witehouse, D. J., Archard, J. F., and Onions, R. A., 1970, "The Properties of Random Surfaces of Significance in Their Contact," Proc. R. Soc. London, Ser. A, **316**, pp. 97–121.
[26] Cooper, M. G., Mikic, B. B., and Yovanovich, M., 1969, "Heat Mass Transfer," Int. J. Heat Mass Transfer, **12**(3), pp. 279–300.
[27] Bowden, F. P., and Tabor, D., 1964, *Friction and Lubrication of Solids*, Clarendon Press, Oxford, UK.
[28] Yovanovich, M., 2006, "Micro and Macro Hardness Measurements: Correlations and Contact Models," AIAA Paper No. 2006–979.
[29] Mikic, B. B., 1974, "Thermal Contact Conductance; Theoretical Considerations," Int. J. Heat Mass Transfer, **17**(2), pp. 205–214.
[30] Sridhar, M. R., and Yovanovich, M., 1996, "Elasto-Plastic Contact Conductance Model for Isotropic Conforming Rough Surfaces and Comparison With Experiments," ASME J. Heat Transfer, **118**(1), pp. 3–9.